Journal of Sound and Vibration (2000) **232**(5), 945–962
doi:10.1006/jsvi.1999.2778, available online at http://www.idealibrary.com on IDEAL®

EXTRACTION OF IMPACTING SIGNALS USING BLIND DECONVOLUTION

J.-Y. Lee and A. K. Nandi

Department of Electrical Engineering and Electronics, The University of Liverpool, Brownlow Hill, Liverpool L69 3GJ, England

(*Received* 22 *April* 1999, *and in final form* 11 *November* 1999)

Two algorithms, the objective function method (OFM) and the eigenvector algorithm (EVA), of the inverse filter estimation are applied to extract the impulsive impacting signals. Both algorithms maximize the estimation of the cumulants with observed data only. The resolution of the reconstructed signals are improved from the observed (measured) signals. Therefore, the "clean" impacting signals can be compared to the known impacting phenomena to determine their origin. The performance of both algorithms are investigated and these appear to perform well.

1. INTRODUCTION

Impacting problems have received attention for over a decade in the field of noise and vibration [1–14]. Researchers were focused on details of impact dynamics, and the methods of bifurcation theory were applied. Rich phenomena were discovered in mathematical models and also validated in experimental models, which included periodic and chaotic chattering. Such knowledge provides the understanding of impacting problems in practice. In industrial applications, such as piping systems, detection and classification of impacting signals from remote sensors are of major interest. Impacting signals, which carry signatures of the condition of a system, normally cannot be measured directly from the impacting sources. In other words, the original impacting signals are modified through propagation and contaminated by unknown noise. In order to monitor system condition, one needs the data from a clear impulsive impact response and the time between impacts. This paper focuses on the examination of the observed signals (measured signals) $z(i)$ from the unknown system $h(l)$ as described in equation (1), where the original signals $x(i)$ are also unknown. The aim is to develop an inverse filter $g(l)$, see equation (2), to reconstruct the impacting signals $y(i)$, i.e., $y(i)$ should approach $x(i)$ as closely as possible. Two existing algorithms, the objective function method (OFM) [15, 16] and the eigenvector algorithm (EVA) [17, 18], for estimation of the coefficients of the inverse filter are applied. Both algorithms are based on higher order statistics [19–22] and only the output signals are required.

In conventional deconvolution, the system and the system's output are known, and the problem is to estimate the input. In blind deconvolution both the system and the system's input are not known, yet the system's input is desired. In such cases, assumptions of a general nature do lead to valid solutions. For example, the fact that the system and the deconvolution filter must be a unit pulse up to a scale factor and delay can be turned into an useful criterion. The EVA [17, 18] is a method of this type. In this particular problem, the

0022-460X/00/200945 + 18 $35.00/0

input (impacting) signals share important properties with the reflection coefficient extraction problem in seismology. These are spiky and sparse time series, and one OFM-type method has been successfully applied [23–26].

The organization of this paper is as follows. In Section 2, two algorithms of the inverse filter estimation are reviewed. In Section 3, three sets of impacting data measured from a cantilever vibrating beam with an inelastic endstop are examined to establish the applicability of the two algorithms. The performance of both algorithms are compared. Further, classification of impacting signals is made from reconstructed signals. In Section 4, the actual impact forces are provided to test the ability of the algorithms. The comparison of the actual forces and the recovered forces are made. Finally, the conclusions are stated in Section 5.

2. REVIEW OF THE METHODS

Using the observed signal $z(i)$ of a linear, time-invariant system $h(l)$, the original signal $x(i)$ is to be recovered by an inverse filter $g(l)$, where a certain time delay and an overall scale factor may be allowed. For a finite impulse response (FIR) model, the system is described as

$$z(i) = \sum_{i=1}^{L} h(l)x(i-l) \tag{1}$$

and the aim is to find an optimal inverse filter $g(l)$ to achieve

$$y(i) = \sum_{i=1}^{L} g(l)z(i-l), \tag{2}$$

where $y(i) \approx \beta x(i-i_0)$ and i, i_0 are integers, β is a scale factor and L is the filter length. Two algorithms, the objective function method (OFM) and the eigenvector algorithm (EVA), are applied in the following investigation; they are based on higher order statistics.

2.1. THE OBJECTIVE FUNCTION METHOD

An objective function with kth order statistics of blind deconvolution to recover the signals with spikes shown in Nandi *et al.* [15] and Lee and Nandi [16] is

$$O_k(g(l)) = \sum_{i=1}^{N} y^k(i) \Big/ \left[\sum_{i=1}^{N} y^2(i) \right]^{k/2}. \tag{3}$$

For comparison with the EVA method, in the next subsection, we set $k = 4$. For more details of this method with $k > 2$, one can refer to references [15, 16]. Optimizing this objective function with respect to the filter coefficient $g(l)$ and using $\partial y(i)/\partial g(l) = z(i-l)$ from equation (2), one gets

$$\left[\sum_{i=1}^{N} y^2(i) \Big/ \sum_{i=1}^{N} y^4(i) \right] \sum_{i=1}^{N} y^3(i)z(i-l) = \sum_{p=1}^{L} g(p) \sum_{i=1}^{N} z(i-l)z(i-p). \tag{4}$$

Equation (4) can be written in matrix from $\mathbf{b} = \mathbf{Ag}$, where $\mathbf{b}$ is a column vector computed from the left-hand side of the equation containing the cross-correlation of the third order

$y(i)$ and $z(i)$. $\mathbf{A}$ is a Toeplitz autocorrelation matrix with dimension $(L \times L)$ containing the autocorrelation of the observed signal $z(i)$, and $\mathbf{g}$ is the column vector of the required coefficients of the inverse filter $g(l)$ for $l = 1$ to L. The algorithm is summarized as below.

Step 1: Set initial optimal filter coefficients $\mathbf{g}^{(0)}$ and Toeplitz autocorrelation matrix $\mathbf{A}$.
Step 2: Compute the output signals $\mathbf{y}^{(0)}$ using the input signal $\mathbf{z}^{(0)}$ and optimal filter coefficients $\mathbf{g}^{(0)}$, i.e., equation (2).
Step 3: Compute the column vector $\mathbf{b}^{(1)}$ using $\mathbf{y}^{(0)}$ and input signal $\mathbf{z}^{(0)}$, i.e., left-hand side of equation (4). Solve new optimal filter coefficients $\mathbf{g}^{(1)} = \mathbf{A}^{-1}\mathbf{b}^{(1)}$.
Step 4: Compute the error criterion

$$\mathbf{e} = (\mathbf{g}^{(1)} - \mu\mathbf{g}^{(0)})/\mu\mathbf{g}^{(0)} \tag{5}$$

and

$$\mu = (E((\mathbf{g}^{(0)})^2)/E((\mathbf{g}^{(1)})^2))^{1/2}, \tag{6}$$

where $E(\cdot)$ is the expected value.

Step 5: If $E(\mathbf{e}) \leqslant 0{\cdot}01$, then stop the process; if $E(\mathbf{e}) > 0{\cdot}01$, then set $\mathbf{g}^{(0)} = \mathbf{g}^{(1)}$ and go to step 2.

2.2. THE EIGENVECTOR ALGORITHM

In the application to communication systems, references [17, 18] and the references therein, an eigenvector method with kurtosis (fourth order statistics) were used to solve the problem of blind equalization. In this paper, it is applied to the current problem of recovering the impacting signals. The criterion is to maximize the cross-cumulant of the output signals $y(i)$ reference signals $r(i)$, i.e.,

$$\text{maximize } |c_4^{yr}(0,0)| \text{ with respect to } r_{yy}(0), \tag{7}$$

where

$$\begin{aligned} c_4^{yr}(0,0) = E\{|y(i)|^2|r(i)|^2\} - [E\{|y(i)|^2\}E\{|r(i)|^2\} \\ + |E\{y^*(i)r(i)\}|^2 + |E\{y(i)r(i)\}|^2] \end{aligned} \tag{8}$$

and $r_{yy}(0)$ is the autocorrelation sequence. By using equation (2) with $y(i) = z(i) \otimes g(l) = z^*g$, where $\otimes$ denotes convolution and * denotes the complex conjugate, equation (7) can be rewritten as

$$\text{maximize } |\mathbf{g}^*\mathbf{C}_4^{zr}\mathbf{g}| \text{ with respect to } \mathbf{g}^*\mathbf{R}_{zz}\mathbf{g}, \tag{9}$$

where $\mathbf{C}_4^{zr}$ is the cross-cumulant matrix $\mathbf{R}_{zz}$ is the autocorrelation matrix, both with dimension $(L \times L)$. The optimization of equation (9) leads to the eigenvector problem

$$\mathbf{C}_4^{zr}\mathbf{g}_{EV} = \lambda\mathbf{R}_{zz}\mathbf{g}_{EV}. \tag{10}$$

The coefficient vector $\mathbf{g}_{Ev}$ is obtained by choosing the eigenvector of $\mathbf{R}_{zz}^{-1}\mathbf{C}_4^{zr}$ associated with the maximum eigenvalue λ. The algorithm is summarized as below.

Step 1: Set initial coefficients $\mathbf{f}^{(0)}$ for the reference system and set iteration $d = 0$ and the total iteration number D.

Step 2: Compute the output signals $\mathbf{r}^{(0)}$ using the input signal $\mathbf{z}^{(0)}$ and reference filter coefficients $\mathbf{f}^{(d)}$. Compute the matrix $\mathbf{R}_{zz}$ and $\mathbf{C}_4^{zr}$

$$\mathbf{R}_{zz} = \frac{1}{N-L}\sum_{k=L}^{N} \mathbf{z}_k \mathbf{z}_k^* \qquad \text{with } \mathbf{z}_k^* = [z(k), z(k-1), \ldots, z(k-L)] \tag{11}$$

and

$$\mathbf{C}_4^{zr} = \frac{1}{N-L}\left(\sum_{k=L}^{N} |r(k)|^2 \mathbf{z}_k \mathbf{z}_k^*\right) - \frac{1}{(N-L)^2}\left[\left(\sum_{k=L}^{N} |r(k)|^2\right)\left(\sum_{k=L}^{N} \mathbf{z}_k \mathbf{z}_k^*\right) + \left(\sum_{k=L}^{N} \mathbf{z}_k r^*(k)\right)\left(\sum_{k=L}^{N} \mathbf{z}_k^* r(k)\right) + \left(\sum_{k=L}^{N} \mathbf{z}_k r(k)\right)\left(\sum_{k=L}^{N} \mathbf{z}_k^* r^*(k)\right)\right]. \tag{12}$$

Step 3: Calculate the most significant eigenvector $\mathbf{g}_{EV}$ of $\mathbf{R}_{zz}^{-1}\mathbf{C}_4^{zr}$.

Step 4: Let $\mathbf{f}^{(d+1)} = \mathbf{g}_{EV}$ and go to step 2 until $d > D$.

3. RESULTS

Three subsections are included in this section. The experimental set-up and simulation results of impacting system are presented in Section 3.1. The criterion of the performance assessment is discussed in Section 3.2, and the measured (observed) signals are examined in Section 3.3 using the OFM and the EVA algorithms. Furthermore, the effect of the additional noise to both algorithms is discussed.

3.1. MEASURED SIGNALS

The observed signals are measured from a vibrating cantilever beam with an inelastic endstop, and the system is driven by harmonic oscillation. The experimental set-up is shown in Figure 1. The simulation results of the impacting response are illustrated in Figure 2, using a bifurcation diagram for a variety of driving frequencies. The results show that the impact resonances occur at 20 and 40 Hz, respectively, and the irregular chattering occurs at the region between these two resonances. The validation of the experimental and simulation results are discussed in references [12–14]. Four types of impacting are characterized in different regions of driving frequency. They are complete chattering (<1 Hz), incomplete chattering (1–10 Hz), periodic chattering (10–25 Hz) and chaotic chattering (26–30 Hz). For more details of the local and global dynamic structures, one can

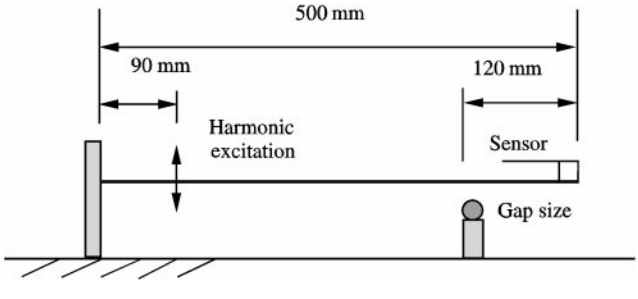

Figure 1. Experimental model of the cantilever beam with an inelastic endstop. The dimension of the aluminium beam is 500 mm × 18 mm × 3 mm.

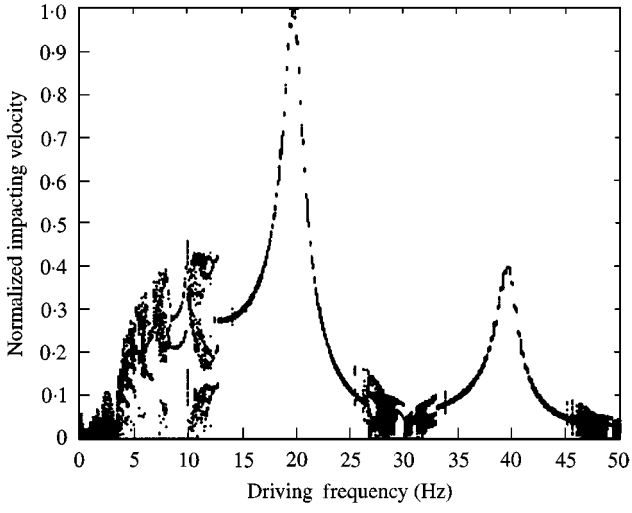

Figure 2. Bifurcation diagram of the cantilever beam with an inelastic endstop (with zero gap size). The solution was plotted by using single-mode summation (numerical data).

refer to references [1–14] and references therein. The data shown in Figures 3(a), 4(a) and 5(a) are normalized acceleration signals (impacting responses) recorded at a sample rate 4000 Hz at different driving frequencies 8, 20 and 28 Hz respectively. The original impacting signals have been propagated through the structure. Therefore, one needs clear impulsive impacting signals to detect and classify the patterns of the original condition. In the following subsections, these observed signals will be processed by the two aforementioned algorithms.

3.2. PERFORMANCE ASSESSMENT

As the assumption in these current problems is that the original impacting signals are unknown, the comparison of the reconstructed signals $y(i)$ to the original signals $x(i)$ is not available. However, the trimmed standard deviation (TSD) of the observed signals and reconstructed signals can be computed. For a given N samples of signal $y(i)$, sort $y(i)$ in increasing order

$$\{Y_i, i = 1, 2, \ldots, N\}, \quad \text{where } Y_1 \leqslant Y_2 \leqslant \cdots \leqslant Y_N \tag{13}$$

and TSD which is defined as

$$TSD = \left[\frac{1}{N-2T}\sum_{i=T+1}^{N-T}(Y_i - TM)^2\right]^{1/2} \tag{14}$$

can be considered as noise in that it is a measure of energy not in the peaks, and the trimmed mean TM is defined as

$$TM = \frac{1}{N-2T}\sum_{i=T+1}^{N-T} Y_i, \tag{15}$$

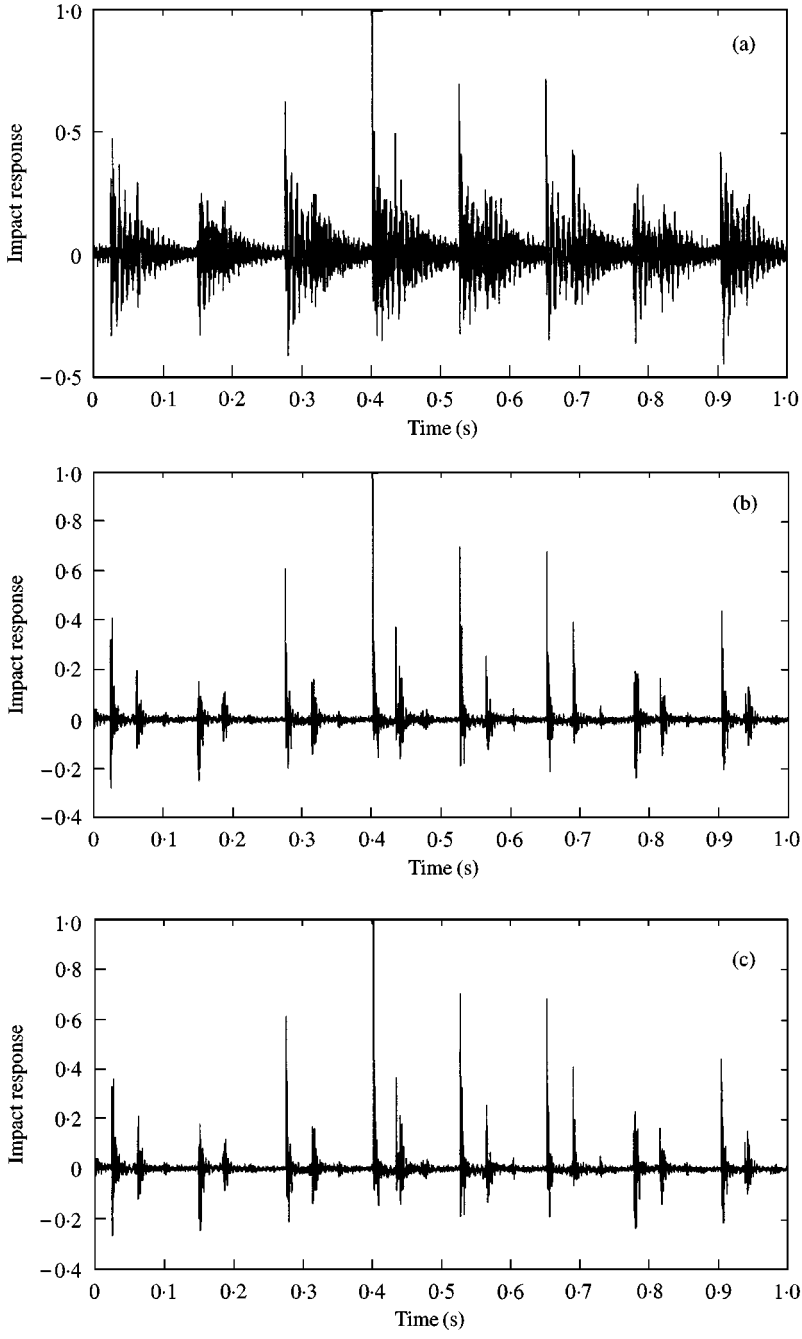

Figure 3. Case 1: 8 Hz driving frequency. (a) The observed signals. (b) The reconstructed signals using the OFM algorithm. (c) The reconstructed signals using the EVA algorithm.

where T is the length of the truncated samples with the nearest integer of γN, where γ is the percent of the highest and lowest data. The coefficient γ can be a complex function due to the reverberation effect and determined by experimental experience. Thus, a small value of TSD indicates a good estimation of inverse filter.

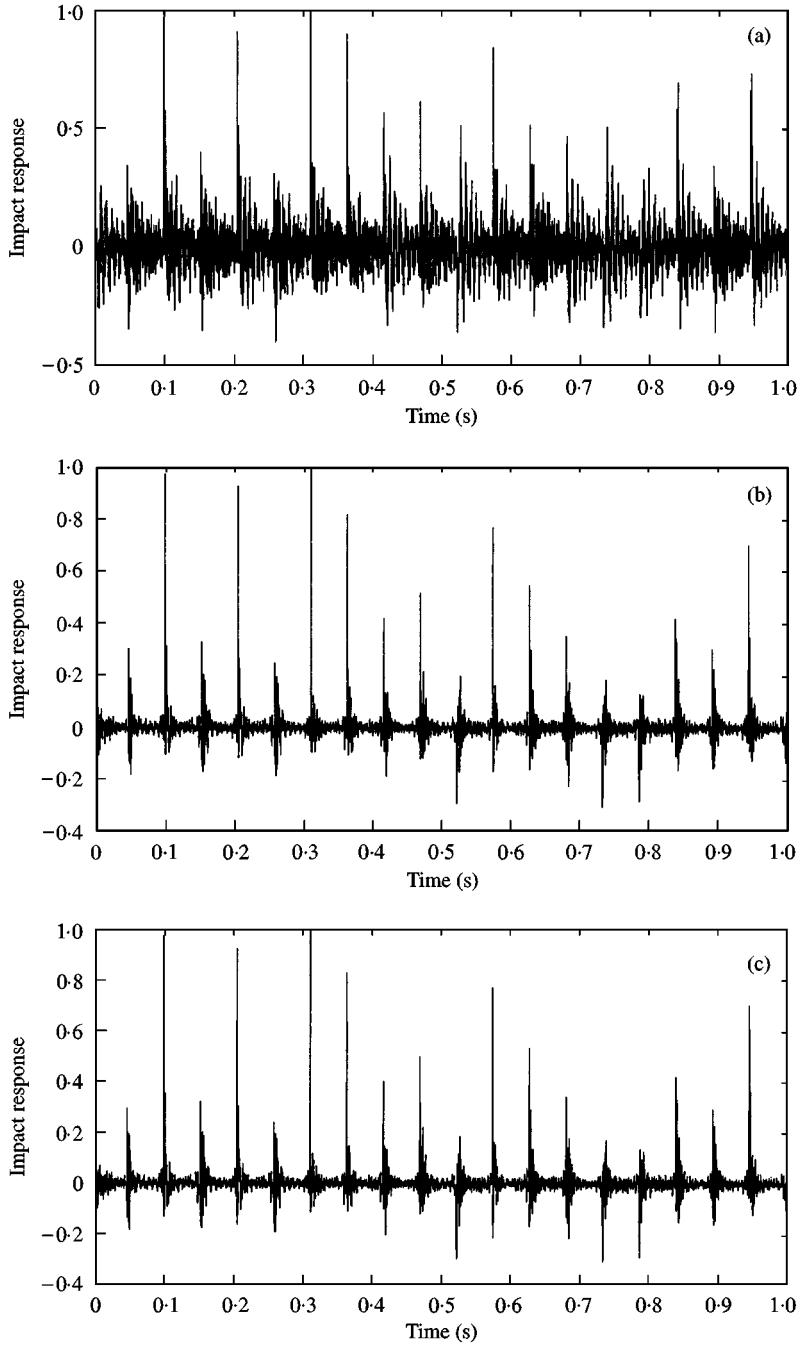

Figure 4. Case 2: 20 Hz driving frequency. (a) The observed signals. (b) The reconstructed signals using the OFM algorithm. (c) The reconstructed signals using the EVA algorithm.

The choice of *TSD* has two advantages as a performance criterion: (1) it can be measured without knowledge of the original signals which is the situation in practical problems, and (2) it brings clear and consistent results when looking at various plots and tables of numbers.

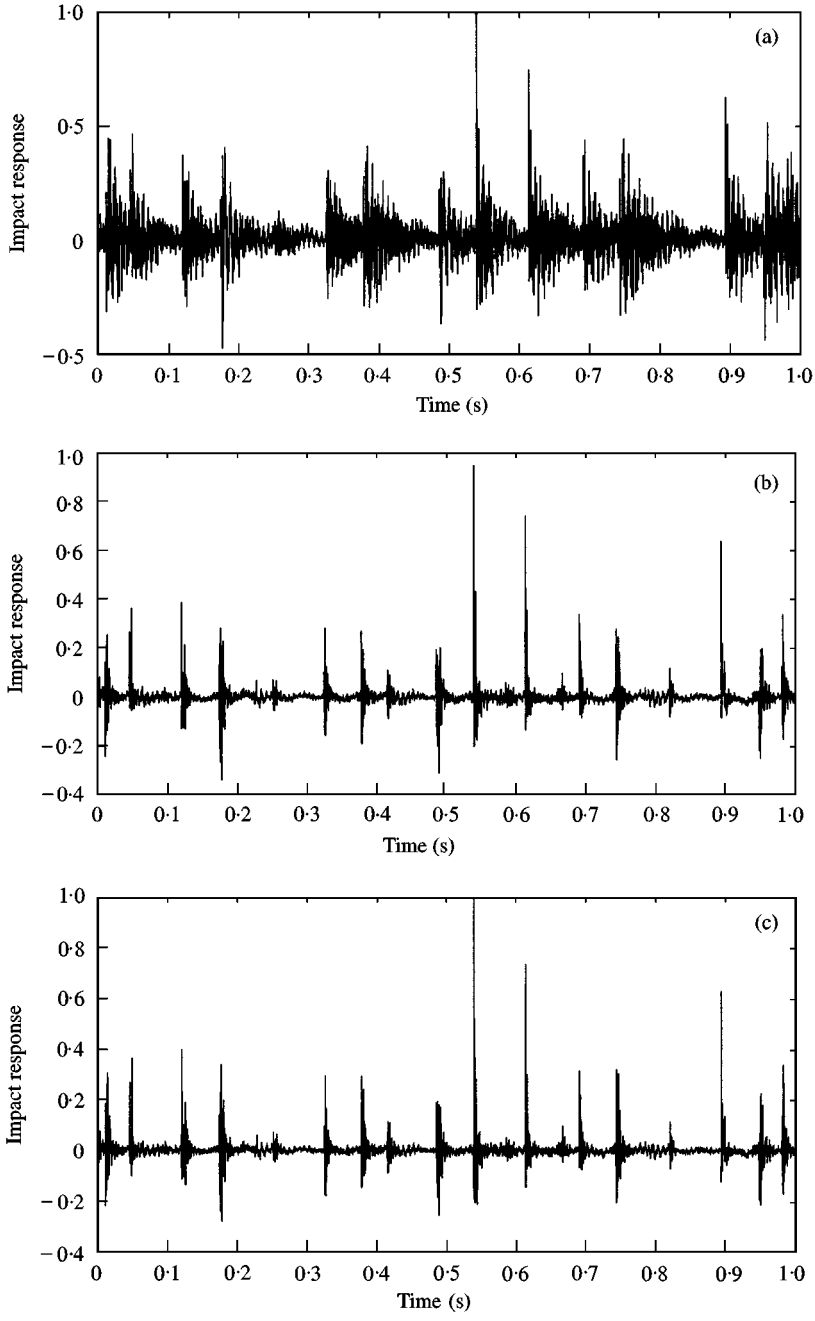

Figure 5. Case 3: 28 Hz driving frequency. (a) The observed signals. (b) The reconstructed signals using the OFM algorithm. (c) The reconstructed signals using the EVA algorithm.

3.3. RECONSTRUCTED SIGNALS

In the following estimation of the inverse filter, the filter length is fixed at 200 and the data length is 4000. The value of the TSD is computed by fixed $\gamma = 0{\cdot}05$ to exclude the largest and smallest spikes, i.e., outliers.

3.3.1. *Case* 1: 8 *Hz driving frequency*

The data shown in Figure 3(a) are the observed signals, and the results shown in Figure 3(b) and 3(c) are the reconstructed signals using the OFM and the EVA algorithm respectively. The resolution of impacting signals are improved by both methods. The values of the TSD for observed signals is 0·056 and for reconstructed signals are 0·011 (OFM) and 0·010 (EVA), shown in Table 1. The results show that the values of TSD (reconstructed) are reduced when compared to the values of TSD (observed). In fact, the impulsive signals are extracted and the contaminated signals are suppressed. The performances shown in Tables 3 (OFM) and 4 (EVA) are computed as

$$\frac{TSD\ (\text{observed}) - TSD(\text{reconstructed})}{TSD(\text{observed})} \times 100\%. \tag{16}$$

Thus, the performance can easily be indicated by a number of percentage. Both algorithms perform well for the observed signals and giving as much as 80·5 (OFM) and 81·6% (EVA) improvement.

Additional artificial Gaussian noise of 10 dB is added to the signals in Figure 3(a) and shown in Figure 6(a). The additional signal-to-noise ratio (SNR) is defined as

$$SNR = 10 \log_{10}(\sigma_z^2/\sigma_n^2), \tag{17}$$

where σ_z^2 is variance of the observed signals and σ_n^2 is additive noise. The results shown in Figure 6(b) and 6(c) are the reconstructed signals from the signals in Figure 6(a). These indicate that the noise floor in Figure 6(b) and 6(c) are higher than Figure 3(b) and 3(c), i.e., the values of TSD, 0·026 (OFM) and 0·031 (EVA), in Table 2 are greater than the values of TSD, 0·011 (OFM) and 0·010 (EVA), in Table 1. This is the effect of the additional noise but as the results show the impacting peaks are extracted correctly. The performances offer 59·7% (OFM) and 51·0% (EVA) improvement from the noisy observed data, see Tables 3 and 4.

3.3.2. *Case* 2: 20 *Hz driving frequency*

The data shown in Figure 4(a) are the observed signals at 20 Hz driving frequency and the reconstructed signals are shown in Figure 4(b) and 4(c) using the OFM and EVA algorithms. The results shown in Figures 7(a)–(c) are with 10 dB additional noise. Referring to Table 1, the value of TSD for observed signals is reduced from 0·076 to 0·018 (OFM) and 0·018 (EVA) for reconstructed signals. With additional noise, see Table 2, the value of TSD is reduced from 0·079 to 0·036 OFM and 0·036 (EVA). The performances offer around 76% improvement for observed signals only and 55% for additional noise data, see Tables 3 and 4.

TABLE 1

The value of TSD: no additional noise

	Observed signals	Reconstructed signals (OFM)	Reconstructed signals (EVA)
Case 1	0·056	0·011	0·010
Case 2	0·076	0·018	0·018
Case 3	0·062	0·013	0·012

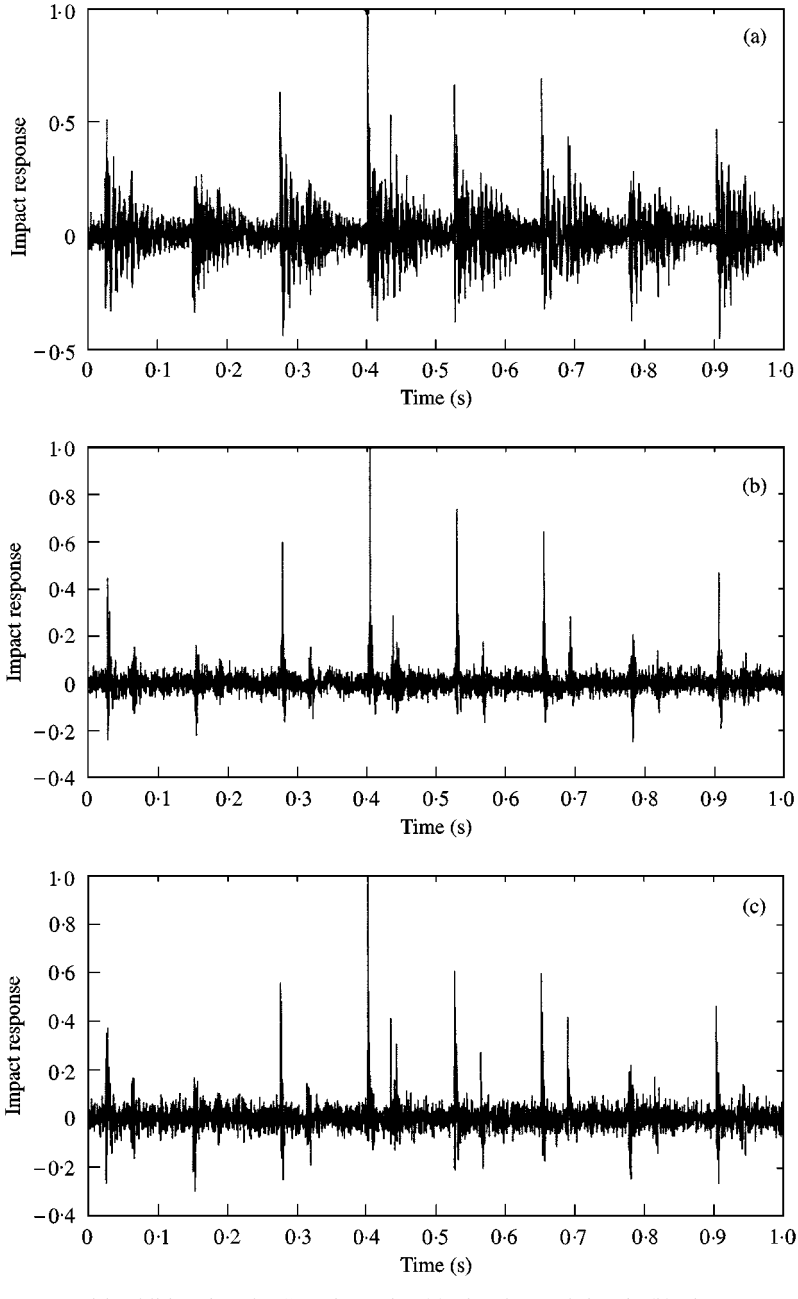

Figure 6. Case 1: With additional 10 dB Gaussian noise. (a) The observed signals. (b) The reconstructed signals using the OFM algorithm. (c) The reconstructed signals using the EVA algorithm.

From the results of the reconstructed signals shown in Figures 3 and 4, i.e., the comparison of the cases 1 and 2, one can see the patterns are different. Both cases are periodic impacting motions, but case 1 has two impacts per period while case 2 has one impact per period. The impacting frequency can be detected from the estimation of the time between impacts using the reconstructed signals. The times between each period of

TABLE 2

The value of TSD: with additional 10 dB *noise*

	Observed signals	Reconstructed signals (OFM)	Reconstructed signals (EVA)
Case 1	0·064	0·026	0·031
Case 2	0·079	0·036	0·036
Case 3	0·071	0·028	0·035

TABLE 3

OFM performance (%)

Additional noise	Case 1	Case 2	Case 3
$SNR = \infty$ dB	80·5	76·1	78·4
$SNR = 10$ dB	59·7	54·9	60·3

TABLE 4

EVA performance (%)

Additional noise	Case 1	Case 2	Case 3
$SNR = \infty$ dB	81·6	76·4	80·1
$SNR = 10$ dB	51·0	54·9	51·2

impacting are 0·124 and 0·052 s for cases 1 and 2 respectively. Thus, the driving frequencies are estimated to be 8·06 and 19·23 Hz which are close to the actual values of 8 and 20 Hz respectively. The motions of these impacting are classified as an incompleted chattering (case 1) and the resonance chattering (case 2) corresponding to Figure 2.

3.3.3. *Case* 3: 28 *Hz driving frequency*

The observed signals of this class motions are shown in Figures 5(a) and 8(a) with additional noise. The reconstructed signals of these two sets of data are shown in Figure 5(b) and 5(c), and Figure 8(b) and 8(c). The improvement of both algorithms are 78·4% (OFM) and 80·1% (EVA) for observed signals only and 60·3% (OFM) and 51·2% (EVA) for additional noise data, see Tables 3 and 4.

The results shown in Figure 5(b) and 5(c) clearly suggest that this class of impacting is not periodic and they are verified as chaotic impacting motions. This disordered impacting vibration may cause a fault alarm and the detection of this problem is important in industrial applications. Compared to case 1 (incomplete chattering) and case 2 (periodic resonance chattering) the exact estimation of driving frequency of this case is not possible because the impact time is irregular. But using the present algorithms, clean spiky signals and the impacting motion with periodic or aperiodic can be distinguished. As the result of case 2 show the impact resonance occurs at 20 Hz in the bifurcation diagram in Figure 2,

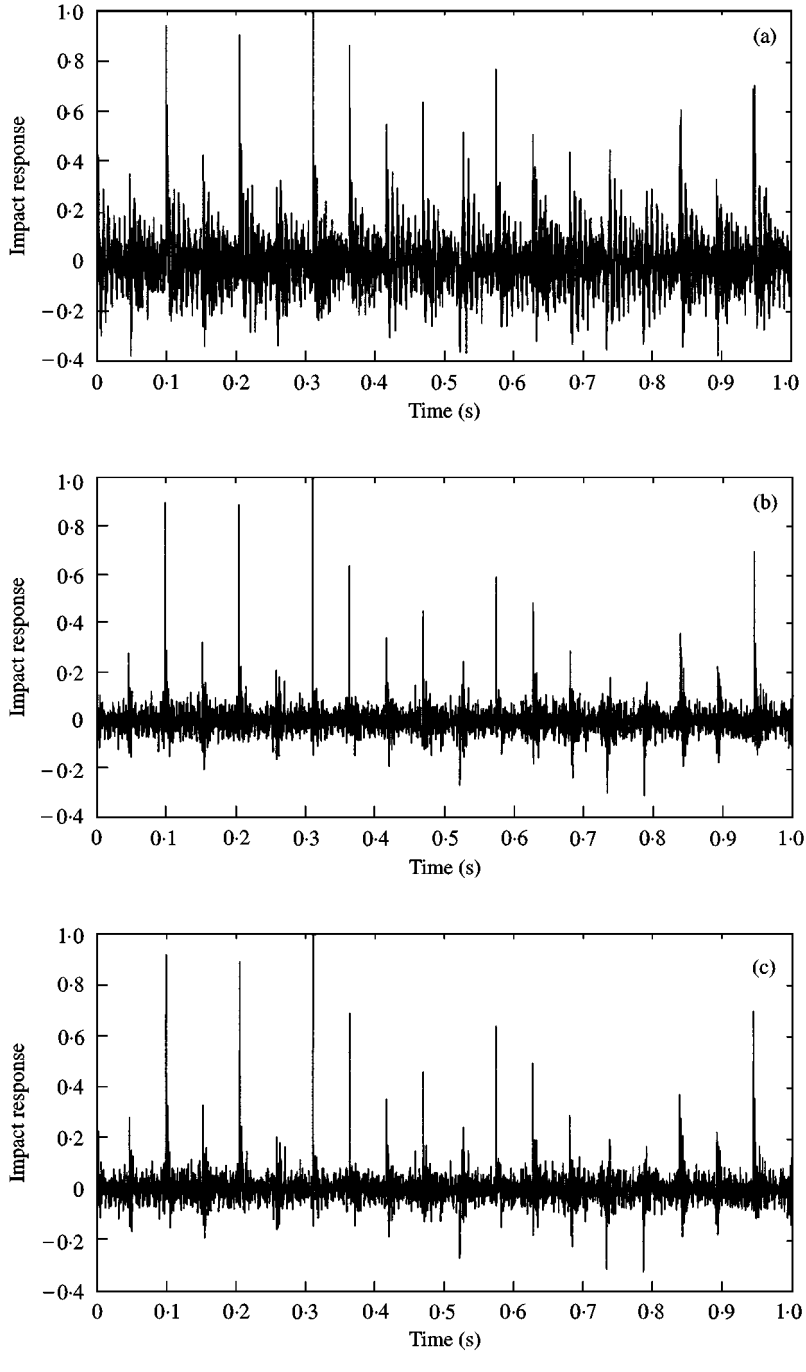

Figure 7. Case 2: With additional 10 dB Gaussian noise. (a) The observed signals. (b) The reconstructed signals using the OFM algorithm. (c) The reconstructed signals using the EVA algorithm.

and the region of chaotic chattering is bounded between periodic chattering at 20 and 40 Hz, i.e., impacting resonance. Therefore, one can estimate the present case in particular region of (26–30) Hz via detecting the periodic chattering in the region of (20–40) Hz.

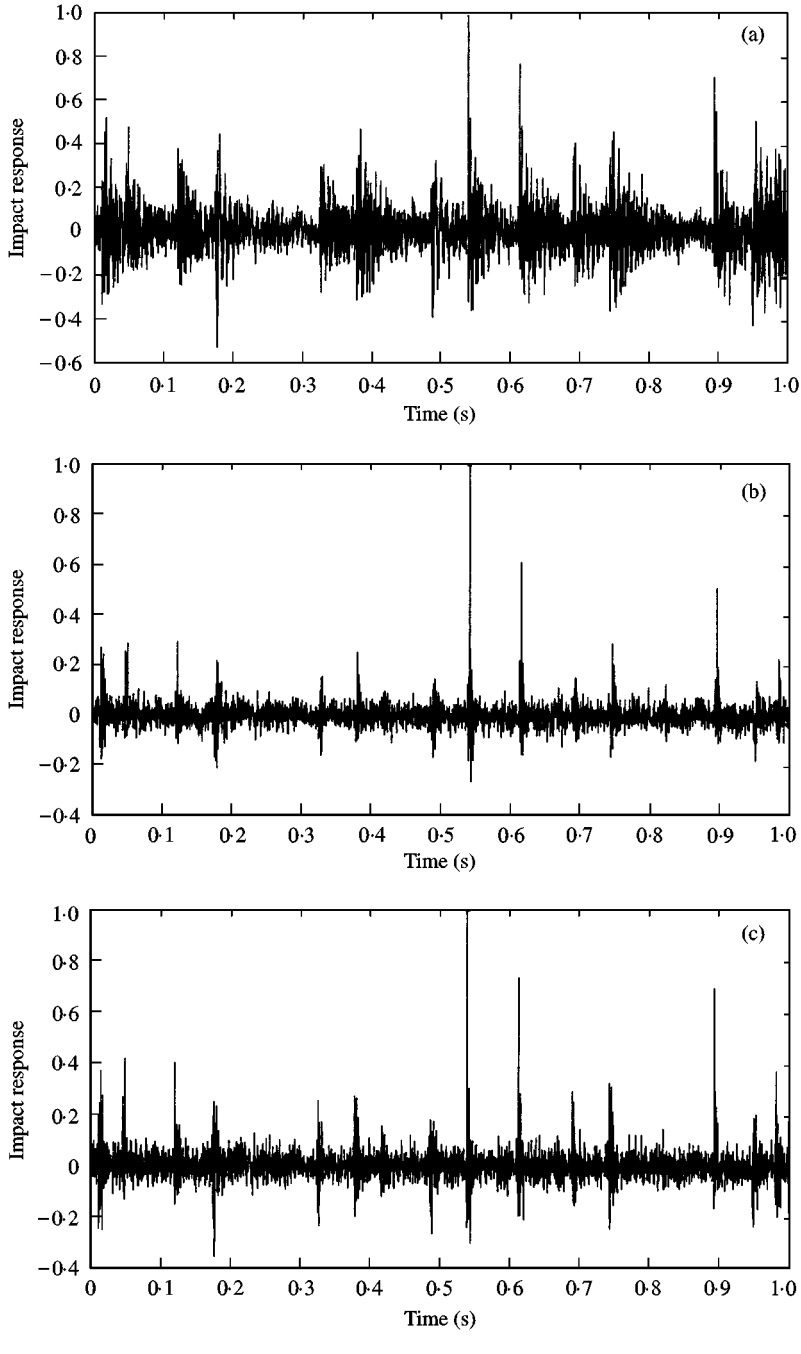

Figure 8. Case 3: With additional 10 dB Gaussian noise. (a) The observed signals. (b) The reconstructed signals using the OFM algorithm. (c) The reconstructed signals using the EVA algorithm.

3.3.4. *The effect of the additional noise*

The principle of both algorithms is to maximize the estimation of the kurtosis, see equations (4) and (7). The effect of this process is to extract relatively larger spikes.

Theoretically, the algorithms are unaffected by the symmetric (Gaussian) noise because the cumulant of this class signals is zero when statistic order is greater than two. But if the additional noise is too high, the original impacting peaks may be buried. In the above examination of the algorithms, with the additional noise of 10 dB they perform well but the improvements are reduced, see Tables 3 and 4. For further noise level of case 1, the sub-impact peaks may be buried. But in case 2 the impact peaks are more significant, thus a higher noise level can be accepted.

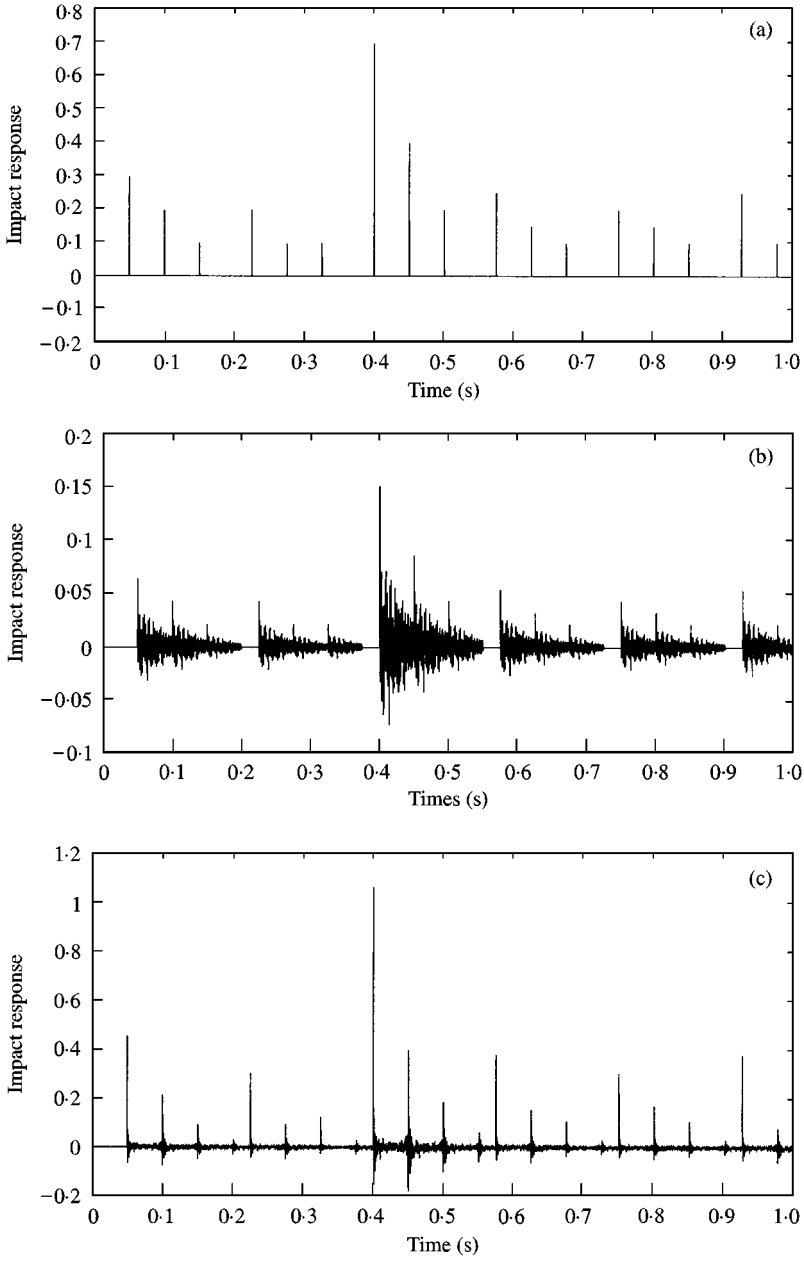

Figure 9. (a) Input signals $\bar{x}(i)$. (b) Output (observed) signals $\bar{z}(i)$. (c) Reconstructed signals $\bar{y}(i)$.

4. DISCUSSION

In the above results, the actual impacting forces cannot be confirmed because the recovered impact forces are compared with the remote measurements. In order to test the

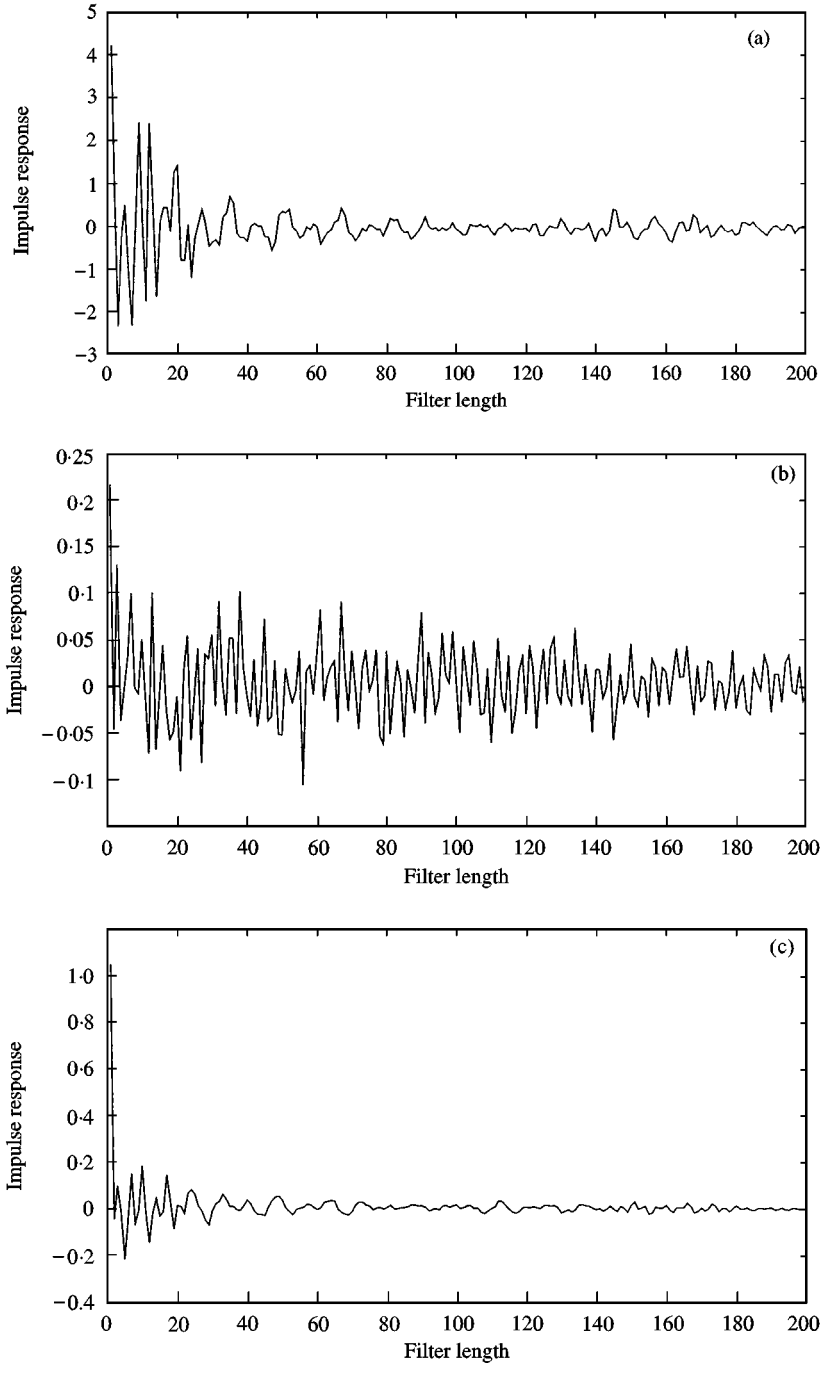

Figure 10. (a) Impulse response of the estimated inverse filter $g(l)$. (b) Impulse response of the estimated system filter $\bar{h}(l)$. (c) The convolution of $\bar{h}(l)$ and $g(l)$. The estimation is based on case 1 data (with 8 Hz driving frequency).

ability of these algorithms to recover impact forces blindly, the original (input) impact forces need to be known. To provide testing and convincing evidence of this, the input forces $\bar{x}(i)$ shown in Figure 9(a) are introduced and the system filter $\bar{h}(l)$ is estimated from the inverse filter $g(l)$. Using the measured data in Figure 3(a) and the OFM scheme, the coefficients of the filter $g(l)$ are estimated and shown in Figure 10(a). By taking the discrete Fourier transform of the series in Figure 9(a), i.e.,

$$G(k) = \sum_{l=1}^{L} g(l) \mathrm{e}^{-\mathrm{j}(2\pi/L)}, \tag{18}$$

where L is the filter length, the coefficients of the filter $\bar{h}(l)$ can be estimated from the inverse Fourier transform of $\bar{H}(k) = 1/G(k)$, i.e.,

$$\bar{h}(l) = \frac{1}{L} \sum_{k=1}^{L} \bar{H}(k) \mathrm{e}^{\mathrm{j}(2\pi/L)}. \tag{19}$$

The resulting impulse response, $\bar{h}(l)$, is shown in Figure 10(b). The convolution result of the filter coefficients $\bar{h}(l)$ and $g(l)$ is shown in Figure 10(c). This unit impulse response confirms that the estimated system filter $\bar{h}(l)$ represents the vibration condition at 8 Hz driving frequency, refer to Section 3.3.1.

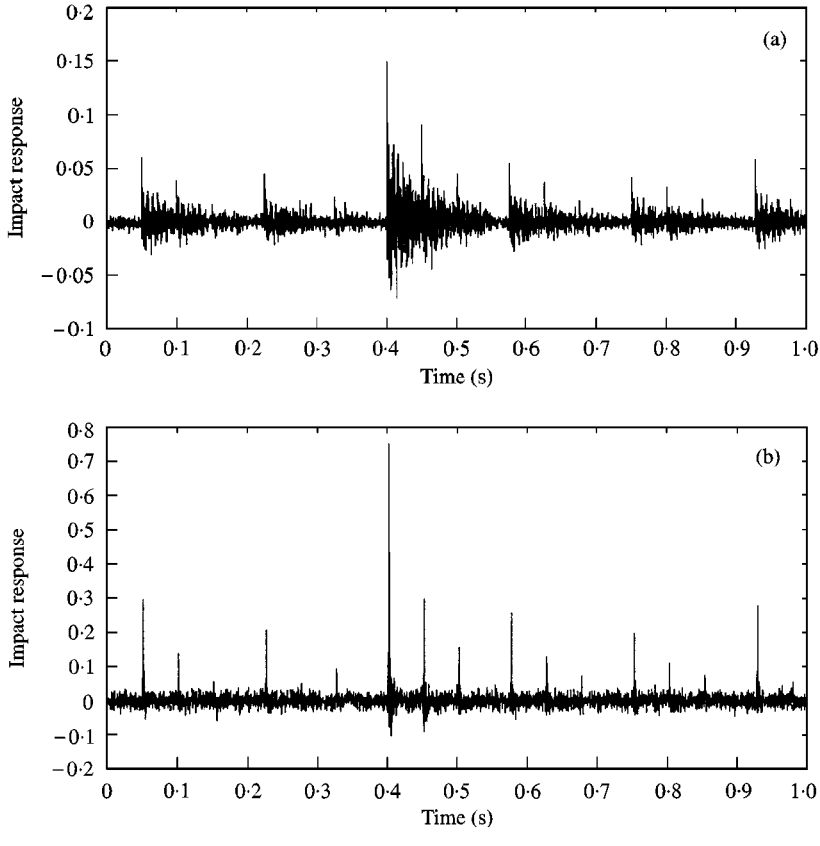

Figure 11. (a) Observed signals $\bar{z}(i)$ with additional 10 dB Gaussian noise. (b) Reconstructed signals.

Applying the simulated input signals $\bar{x}(i)$ in Figure 9(a) to the estimated system filter $\bar{h}(l)$, the output ("observed") signals $\bar{y}(i)$ are shown in Figure 9(b). Following the blind deconvolution scheme of the OFM, the reconstructed signals are shown in Figure 9(c). Same as in the previous results, clear impacting signals are recovered. The difference of the actual input signals $\bar{x}(i)$ and the reconstructed signals $\bar{y}(i)$ can be computed as a value of the standard deviation (*SD*),

$$SD = \left[\frac{1}{N} \sum_{i=1}^{N} (\bar{y}(i) - \bar{x}(i))^2 \right]^{1/2}. \tag{20}$$

Therefore, small value of *SD* indicates a good estimation of the inverse filter. The value of *SD* for Figure 9(a) and 9(c) is 0·014 while the value of TSD (equation (14)) for Figure 9(c) is 0·010. Added additional 10 dB Gaussian noise to Figure 9(b) the results shown in Figure 11(a) are simulated "observed" signals, and the reconstructed signals are shown in Figure 11(b). The value of *SD* for Figures 9(a) and 11(b) is 0·027 and the value of TSD for Figure 11(b) is 0·016. In the comparison of the values *SD* (the input forces are known) and TSD (the input forces are unknown), the results show that they consistently indicate the performance of the algorithm well.

5. CONCLUSION

Two algorithms based on higher order statistics were applied to extract the impulsive impact responses. Consequently, the reconstructed signals can be compared to the known impacting phenomena to determine their origin. Various impacting problems can be classified using the observed signals only. The performance of both algorithms are examined and these perform well. The ability of the algorithms are also validated by the comparison of the simulated input forces and the reconstructed forces, and the assessment criterion shows that the values of TSD (blind) is a consistent indicator of the trend of the values of *SD* (non-blind).

ACKNOWLEDGMENT

The authors would like to acknowledge the valued comments made by the anonymous reviewers and the financial support of the Engineering and Physical Science Research Council of U.K. under the research grant no. GR/K99787.

REFERENCES

1. S. W. SHAW and P. J. HOLMES 1983 *Journal of Sound and Vibration* **90**, 129–155. A periodically forced piecewise linear oscillator.
2. S. W. SHAW 1985 *Journal of Sound and Vibration* **99**, 199–212. Forced vibrations of a beam with one-sided amplitude constraint: theory and experiment.
3. G. S. WHISTON 1987 *Journal of Sound and Vibration* **115**, 303–319. The vibro-impact response of a harmonically excited and preloaded one-dimensional linear oscillator.
4. G. S. WHISTON 1987 *Journal of Sound and Vibration* **118**, 395–429. Global dynamics of a vibro-impacting linear oscillator.
5. A. B. NORDMARK 1991 *Journal of Sound and Vibration* **145**, 279–297. Non-periodic motion caused by grazing incidence in an impact oscillator.
6. G. S. WHISTON 1992 *Journal of Sound and Vibration* **152**, 427–460. Singularities in vibro-impact dynamics.

7. F. PETERKA and J. VACIK 1992 *Journal of Sound and Vibration* **154**, 95–115. Transition to chaotic motion in mechanical systems with impacts.
8. A. IVANOV 1993 *Journal of Sound and Vibration* **162**, 562–565. Stabilization of an impact oscillator near grazing incidence owing to resonance.
9. W. FANG and J. A. WICKERT 1994 *Journal of Sound and Vibration* **170**, 397–409. Response of a periodically driven impact oscillator.
10. A. IVANOV 1994 *Journal of Sound and Vibration* **178**, 361–378. Impact oscillations: linear theory of stability and bifurcations.
11. C. BUDD and F. DUX 1995 *Journal of Sound and Vibration* **184**, 475–502. The effect of frequency and clearance variations on single-degree-of-freedom impact oscillators.
12. J.-Y. LEE and J. K. HAMMOND 1995 *Proceeding of 2nd International Conference on Acoustical and Vibratory Surveillance Methods and Diagnostic Techniques*, 495–505. Characterization of mechanical vibrating systems with internal impacts.
13. J.-Y. LEE and J. K. HAMMOND 1997 *Proceedings of the 6th International Conference on Recent Advances in Structural Dynamics, Southampton University*, Vol. 1, 773–783. Safe design of impacting systems.
14. J.-Y. LEE 1997 *Ph.D. thesis, ISVR, Southampton University, U.K.* Characterization and suppression of chattering in impacting structures.
15. A. K. NANDI, D. MAMPEL and B. ROSCHER 1997 *IEEE Transactions on Signal Processing* **45**, 1382–1389. Blind deconvolution of ultrasonic signals in non-destructive testing applications.
16. J.-Y. LEE and A. K. NANDI 1998 *Mechanical Systems and Signal Processing* **12**, 357–371. Blind deconvolution of impacting signals using high order statistics.
17. B. JELONNEK and K.-D. KAMMEYER 1994 *Signal Processing* **36**, 251–259. A closed form solution to blind equalization.
18. B. JELONNEK, D. BOSS and K.-D. KAMMEYER 1997 *Signal Processing* **61**, 237–264. Generalized eigenvector algorithm for blind equalization.
19. J. M. MENDEL 1991 *Proceedings of IEEE* 79, 278–305. Tutorial on higher order statistics in signal processing and system theory: theoretical results and some applications.
20. C. L. NIKIAS and J. M. MENDEL 1993 *IEEE Signal Processing Magazine* **10**, 10–37. Signal Processing with high-order spectra.
21. A. K. NANDI 1998 *Signal Analysis and Prediction* (A. Prochazka, J. Uhlir, P. J. W. Rayner and N. G. Kingsbury, editors) 57–77. Higher order statistics in signal processing.
22. A. K. NANDI 1999 *Blind Estimation using Higher-order Statistics*. Dordrecht: Kluwer Academic Publishers.
23. A. T. WALDEN 1985 *Geophysics* **50**, 2862–2888. Non-Gaussian reflectivity, entropy and deconvolution.
24. R. W. WIGGINS 1978 *Geoexploration* **16**, 21–35. On minimum entropy deconvolution.
25. D. DONOHO 1981 *Applied Time Series II*, 565–608. On minimum entropy deconvolution.
26. C.-Y. CHI and M.-C. WU 1995 *Signal Processing* **43**, 55–63. Inverse filter criteria for blind deconvolution and equalization using two cumulants.